ELSEVIER

www.elsevier.nl/locate/jorganchem

Journal of Organometallic Chemistry 596 (2000) 252–256

Journal of Organometallic Chemistry

Note

Formation of a Pt_1Sn_1(niggliite)–silica xerogel nanocomposite using a PtSn (1:1) organometallic precursor

Joseph P. Carpenter [a], C.M. Lukehart [a,*], S.R. Stock [b]

[a] *Department of Chemistry, Vanderbilt University, Nashville, TN 37235, USA*
[b] *School of Materials Science and Engineering, Georgia Institute of Technology, Atlanta, GA 30332, USA*

Received 15 August 1999; received in revised form 10 November 1999

Abstract

Covalent incorporation of a complex containing a bifunctional thiolate substituent and a 1:1 Pt:Sn metal core stoichiometry into a silica xerogel matrix is accomplished using sol–gel processing. Thermal degradation of this complex–silica xerogel composite under solely reducing conditions affords a nanocomposite material in which the nanocluster phase has the Pt_1Sn_1 composition of niggliite. The use of a PtSn (1:1) complex as a single-source molecular precursor for the formation of a Pt_1Sn_1–silica xerogel nanocomposite is demonstrated.

Keywords: Nanocomposites; Nanoparticles; Silica xerogels; Sol–gel chemistry; Niggliite

1. Introduction

We have recently reported a 'molecules-to-nanocomposite' synthetic strategy, whereby precursor complexes containing appropriate bifunctional ligands are covalently incorporated into silica xerogels using sol–gel chemistry and are then degraded to form a nanocomposite material. The composition of the nanocluster phase is controlled through variation of the metal and ligand elemental stoichiometries of the molecular precursor. Silica xerogel nanocomposites containing nanoclusters of various metals, metal oxides, metal phosphides, elemental germanium, and the known cobalt carbide, Co_3C, have been prepared using this method [1].

Given the importance of binary intermetallic and alloy compositions in chemical catalysis [2,3], the general scope of this synthetic method would be greatly expanded if mixed-metal–silica xerogel nanocomposites could be formed from single-source molecular precursors with control over the relative stoichiometry of the metals. A Pt–Sn target nanocluster composition was chosen because Pt and Sn form intermetallic phases instead of alloys. Each of the five known Pt–Sn intermetallic compounds (Pt_3Sn, PtSn, Pt_2Sn_3, $PtSn_2$, and $PtSn_4$) has a distinct X-ray diffraction (XRD) pattern, so any phase separation that might occur upon conversion of a precursor–silica xerogel to a nanocomposite material should be readily detected.

In addition, Pt–Sn phases exhibit much chemistry of interest. The surface chemistry of Pt–Sn compositions has been a topic of several recent reports [4], and supported nanoparticulate Pt–Sn compositions are widely studied for their catalytic activity and are used as commercial catalysts in hydrocarbon reforming and isobutane dehydrogenation [5]. Pt–Sn catalysts are usually supported on ceramic supports, such as silica or alumina, and the desired metal stoichiometry is achieved by proper mixing of separate Pt and Sn reagents. While some such syntheses yield a single-phase of Pt and Sn [5b], the formation of a mixture of Pt–Sn phases is more commonly observed [5d–f]. While Pt–Sn bimetallic complexes have been used as supported molecular catalysts [6], such complexes might also serve as bimetallic precursors for the formation of nanoparticulate Pt–Sn phases of controlled stoichiome-

* Corresponding author.

0022-328X/00/$ - see front matter
PII: S0022-328X(99)00697-X

try. We now report the detailed synthesis and characterization of a Pt_1Sn_1–silica xerogel nanocomposite using a PtSn (1:1) bimetallic complex as a single-source molecular precursor. An overview of this synthetic strategy has already appeared [1a].

2. Experimental

2.1. General synthesis and characterization methods

The reagents, tetramethylorthosilicate (TMOS) and (3-mercaptopropyl)trimethoxysilane, were purchased from Aldrich. The compound *cis*-$Pt(Ph)(Ph_3P)_2(SnPh_2Cl)$ was prepared according to literature procedures [7].

Proton and ^{31}P-NMR spectra were recorded on a IBM NR-300 spectrometer (300 MHz) using the ^2H signal of the solvent as an internal lock frequency. Chemical shifts (in δ) were measured with respect to the residual solvent peak as an internal standard.

Electron microscopic data were obtained using a Philips CM20T transmission electron microscope (TEM) operating at 200 kV. Samples for the TEM were prepared by dispersing a powdered sample of nanocomposite onto a 3 mm diameter copper grid covered with amorphous holey carbon as a substrate. These samples were analyzed with standard bright-field (BF) imaging for particle size distribution, selected area diffraction (SAD) for their crystal structures, and X-ray energy dispersive spectroscopy (EDS) for semi-quantitative chemical composition.

X-ray diffraction (XRD) scans were obtained using a Philips PW1800 $\theta/2\theta$ automated powder diffractometer equipped with a Cu target and a post-sample monochromator. Samples for XRD were prepared by placing a uniform layer of powdered nanocomposite onto double-sided tape affixed to the sample holder. The sample area was greater than the ca. 1×1 cm^2 area irradiated by the X-ray beam. Considerable caution was used to keep the top of the sample surface flat and coplanar with the diffractometer rotation axis. Prior to peak width measurement, each diffraction peak was corrected for background scattering and was stripped of the Kα2 portion of the diffracted intensity. In suitable samples, the full width at half maximum (FWHM) was measured for each peak. Crystallite size, L, was calculated from Scherrer's equation, $L = K\lambda/\beta \cos\theta_B$, for peak broadening from sized effects only (where β is the peak FWHM measured in radians on the 2θ scale, λ is the wavelength of X-rays used, θ_B is the Bragg angle for the measured *hkl* peak, and K is a constant equal to 1.00 for L taken as the volume-averaged crystallite dimension perpendicular to the *hkl* diffraction plane [8]).

Chemical microanalyses were performed by Galbraith Laboratories, Inc., Knoxville, TN.

2.2. Synthesis of $(Ph_3P)_2Pt(Ph)[Ph_2SnS(CH_2)_3Si(OCH_3)_3]$ (1)

To a solution of $(Ph_3P)_2Pt(Ph)(SnPh_2Cl)$ (196.3 mg, 0.178 mmol) in 10 ml of CH_2Cl_2 was added NaI (133 mg, 0.89 mmol) dissolved in 6 ml of acetone. After stirring for 10 min, a mixture of $HS(CH_2)_3Si(OMe_3)_3$ (0.04 ml, 0.214 mmol) and NEt_3 (0.03 ml, 0.22 mmol) dissolved in 8 ml of CH_2Cl_2 and 5 ml of acetone was added dropwise over a period of 10 min to the cloudy solution. The slightly opaque yellow solution was stirred for 30 min, and then the solvent was removed at reduced pressure to give a crude yellow solid. This residue was extracted with 5×10 ml of 4:1 hexane–benzene, and the resulting extracts were filtered through Celite. The solvent was removed from the filtrate at reduced pressure to give a pale yellow oil. The product was obtained as a pale yellow crystalline solid upon crystallization from ether–hexane at -30°C. The crystalline solid was collected, washed with 3×10 ml of hexane and dried in vacuo for 30 min (134 mg, 60%, **1**): ^1H-NMR (300 MHz, $CDCl_3$): δ 0.19 (m, 2H, $SiCH_2$), 1.05 (m, 2H, CH_2CH_2 CH_2), 1.75 (t, 2H, SCH_2, $^3J_{SnH} = 32$ Hz), 3.35 (s, 9H, OCH_3), 6.34 (m, 2H, PtPh), 6.90–7.60 (m, 43H, PPh, SnPh, and PtPh). $^{31}P\{^1H\}$-NMR ($CDCl_3$): δ 19.0 (d, 1, $^2J_{PPtP} = 15$, $^1J_{PPt} = 2059$, $^2J_{PPtSn} = 159$ Hz), 24.2 (d, 1, $^2J_{PPtP} = 15$, $^1J_{PPt} = 2501$, $^2J_{PPtSn(117)} = 2047$, $^2J_{PPtSn(119)} = 2142$ Hz). ^1H-NMR spectra of compound **1** reveal additional methoxy singlets of very low intensity in the range δ 3.3–3.6, presumably due to trace amounts of impurities arising from hydrolysis and/or condensation reactions of the reactive $Si(OMe)_3$ group. Anal. Calc. C, 56.97; H, 4.78. Found: C, 55.92; H, 5.65%.

2.3. Covalent incorporation of 1 into a silica xerogel (2)

A vial was charged with 74 mg of **1** and the solid was dissolved in 1.0 ml of THF. To this solution was added TMOS (0.25 ml, 1.7 mmol) and water (0.31 ml, 17 mmol). Addition of 0.25 ml of THF to the resulting dispersion produced a homogeneous pale yellow solution, and 0.05 ml of 0.158 M HNO_3 was added as a hydrolysis catalyst. After 24 h gelation had occurred to give a bright yellow xerogel. This xerogel composite was washed with 3×10 ml of THF and then dried in vacuo for 30 min to give 166 mg of **2**.

2.4. Thermal decomposition of **2** to give a Pt_1Sn_1–silica xerogel nanocomposite (**3**)

To an alumina crucible was added 20.4 mg of the precursor–silica xerogel composite **2**. The crucible assembly was inserted into a quartz tube centered within a tube furnace. The quartz tube was purged with hydrogen (150 ml per min) for several minutes at room temperature (r.t.), and then the sample was heated at a rate of ca. 15° per min to a temperature of 700°C. Heating was continued for 2 h, and then the sample was cooled to r.t. under a flow of hydrogen gas, affording 14.7 mg of the black nanocomposite **3a**. This nanocomposite contained Pt_1Sn_1 (niggliite) nanoclusters having an average diameter of 6.0 nm. To facilitate unambiguous characterization of the nanocluster phase, nanocomposite **3b** was prepared at a higher temperature to afford larger Pt_1Sn_1 nanoclusters. A 23.3 mg sample of the precursor–silica xerogel composite **2** was heated under a hydrogen atmosphere to 900°C and was held at that temperature for 1 h. Upon cooling to r.t., 15.4 mg of nanocomposite **3b** was isolated as a black solid. This nanocomposite contained Pt_1Sn_1 (niggliite) nanoclusters having an average diameter of 12.0 nm.

3. Results and discussion

Pt_1Sn_1 was chosen as a specific target composition to demonstrate that mixed-metal–silica xerogel nanocomposites of controlled metal stoichiometry can be prepared using single-source molecular precursors. Nanoclusters of the Pt_1Sn_1 intermetallic compound, known as niggliite, are recognized catalysts [5], and this composition is one of the two congruently melting phases present in the Pt–Sn phase diagram [9]. Congruently melting phases should be less prone to undergo phase separation at the solid–liquid phase transition, which can be important in nanocluster syntheses since many substances exhibit reduced melting points at the nanoscale.

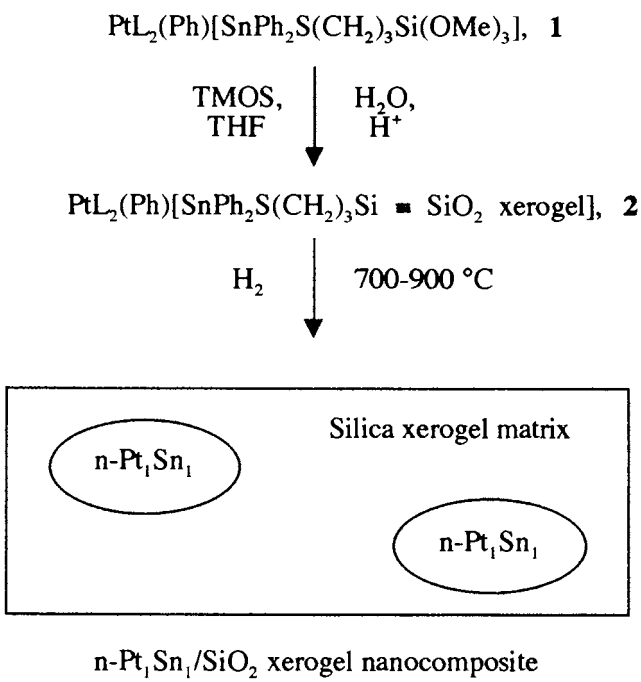

Scheme 1. Preparation of the niggliite–silica xerogel nanocomposites **3a** and **3b**.

Complex **1** contains a 1:1 Pt:Sn stoichiometry and was selected as a single-source precursor suitable for niggliite nanocluster formation. As shown in Eq. (1), halide exchange of the chloro substituent of *cis*-$(Ph_3P)_2Pt(Ph)(SnPh_2Cl)$ by iodide occurs as a first step [7], and facile nucleophilic displacement of iodide by the desired bifunctional thiolate group proceeds smoothly in a second step to give **1**. Direct displacement of chloride by the thiolate group is too slow to be useful. Complex **1** is isolated by crystallization as a pale yellow solid of good purity, along with trace contaminants probably resulting from partial hydrolysis and/or condensation of the Si–OMe groups. Chromatography on ceramic supports must be avoided because of the presence of the highly reactive $Si(OMe)_3$ group. The *cis* structure of **1** is confirmed by its ^{31}P-NMR spectrum, which exhibits two doublets for the non-equivalent phosphorus nuclei and a $^2J_{PP}$ coupling constant of 15 Hz. The expected platinum and tin satellites are also observed for these resonances. Connectivity between the thiolate group and the Sn atom is confirmed by observing a $^3J_{SnH}$ coupling constant of 32 Hz. Typical values of $^3J_{SnH}$ coupling in related (monothiolato)organotin compounds range from 33 to 38 Hz [10].

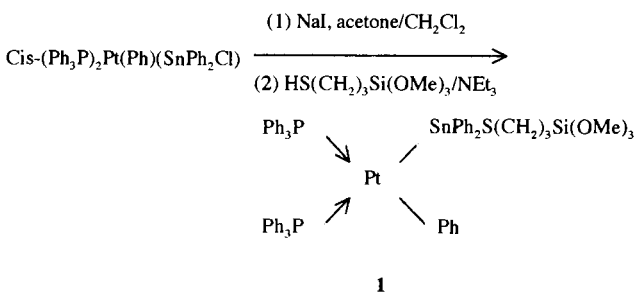

(1)

Complex **1** is readily soluble in aqueous THF solutions containing TMOS. Addition of catalytic amounts of aqueous nitric acid to such solutions initiates hydrolysis of the Si–OMe groups of both TMOS and of complex **1**. Sol-gel heterocondensation of these Si–OH intermediates leads to homogeneous covalent incorporation of **1** into a silica xerogel matrix as it is being formed [11], as shown in Scheme 1. For this reason, complexes containing pendant (alkoxy)silyl functionalities, like **1**, serve as ideal molecular precursors for

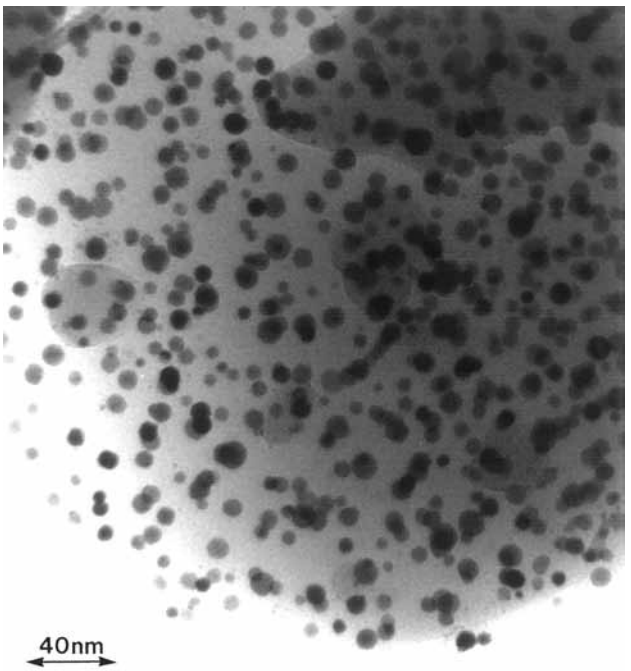

Fig. 1. TEM micrograph of the Pt_1Sn_1–silica xerogel nanocomposite **3b**.

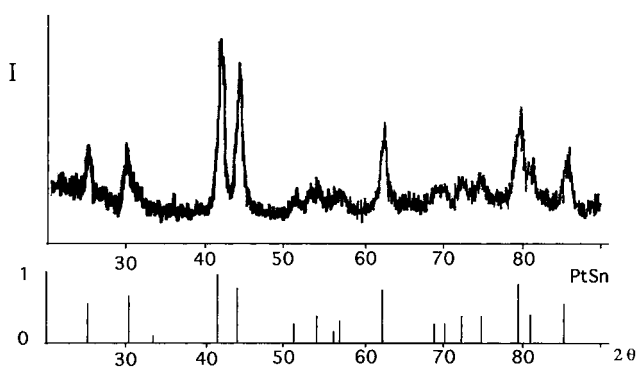

Fig. 2. XRD scan of the Pt_1Sn_1–silica xerogel nanocomposite **3b** (upper scan) along with the standard XRD line pattern (PDF card no. 25-614) of pure Pt_1Sn_1(niggliite) both recorded with Cu–K_α radiation.

nanocomposite materials prepared through sol–gel processing. The resulting yellow precursor–silica xerogel composite, *cis*-$(Ph_3P)_2Pt(Ph)[SnPh_2S(CH_2)_3Si{\equiv}$silica xerogel, **2**, can be washed without extraction of the precursor and is obtained as a bright yellow xerogel powder.

Thermal treatment of the precursor–silica xerogel composite **2** under a hydrogen atmosphere at 700°C for 2 h or at 900°C for 1 h affords black xerogels **3a** or **3b**, respectively, see Scheme 1. The loading level of precursor complex was arbitrarily chosen to give xerogels containing ca. 15 wt.% total metal.

TEM micrographs of xerogel **3a** reveal crystalline nanoclusters highly dispersed throughout the xerogel matrix. Diameters of the nanoclusters range from 2 to 15 nm with a monomodal particle size distribution. An EDS spectrum confirms the presence of Pt, Sn and Si with no other elements detected. SAD electron diffraction patterns show three rings that can be indexed using the cell parameters known for the hexagonal Pt_1Sn_1 niggliite [*hkl*, *d*(obsd), *d*(niggliite): 012, 2.13, 2.157 Å; 110, 2.05, 2.050 Å; 022, 1.49, 1.485 Å]. An XRD scan of this nanocomposite shows a peak near 22° 2θ arising from amorphous scattering from the silica xerogel host matrix and several very broad peaks at 2θ values corresponding to XRD peaks known for pure niggliite. The average diameter of the crystalline nanoclusters is 6.0 nm as calculated from the widths of the 012 and 110 XRD peaks. The presence of other crystalline phases is not evident. These data strongly indicate that the nanocrystalline phase present within this nanocomposite has the Pt_1Sn_1 niggliite composition and structure. This composition is precisely that of the metal stoichiometry found in complex **1**.

To verify more clearly that this nanocomposite contains nanoclusters of niggliite and that phase separation of the metals has not occurred during thermal treatment, the nanocomposite was prepared at higher temperature, **3b**. These conditions afforded slightly larger crystalline nanoclusters that are more clearly characterized by diffraction methods. A TEM micrograph of nanocomposite **3b** is shown in Fig. 1. The high contrast of the observed nanoclusters indicates high crystallinity relative to the amorphous silica xerogel matrix. Some nanocrystals are properly oriented with respect to the electron beam that corners and edges and even nearly hexagonal projections are evident. This latter observation is consistent with the known hexagonal crystal structure of niggliite. A histogram of nanocluster particle sizes shows particle diameters ranging from 3 to 15 nm with a majority of particles having diameters greater than 10 nm. A monomodal particle size distribution is observed. An EDS spectrum shows emission from Pt, Sn and Si with no evidence of the presence of phosphorus or sulfur.

Five rings are observed in the SAD electron diffraction pattern of nanocomposite **3b**. Each ring can be indexed using the cell parameters of niggliite [*hkl*, *d*(obsd), *d*(niggliite): 001, 2.99, 2.971 Å; 012, 2.13, 2.157 Å; 110, 2.05, 2.050 Å; 022, 1.49, 1.485 Å; 122, 1.20, 1.203 Å]. Furthermore, electron diffraction from a single nanocrystal gives a spot pattern consisting of at least 30 spots. Several of the most prominent spots have been indexed using the cell constants known for niggliite.

The most definitive evidence supporting the selective formation of niggliite nanocrystals is revealed in the XRD scan of nanocomposite **3b**, as shown in Fig. 2. Diffraction peaks are observed at the proper 2θ values and with the expected relative intensities, as expected for diffraction from pure niggliite. Any crystalline im-

purity or other phase that might be present must be present as a very minor component. From the widths of the 012 and 110 peaks, the average diameter of the niggliite nanoclusters is calculated to be 12.0 nm. Although five different Pt–Sn compositions are present in the Pt–Sn phase diagram, only nanoclusters of PtSn are formed when complex **1** is used as a single-source precursor. Successful formation of Pt_1Sn_1 nanoparticles from a PtSn (1:1) bimetallic precursor bound to a silica xerogel matrix demonstrates synthetic control of the elemental composition and stoichiometry of a bimetallic nanocluster material through proper choice of the metal content of a molecular precursor.

Thermal treatment of the precursor–silica xerogel composite **2** at 700°C for 1 h in air, followed by 2 h in hydrogen, gives a black nanocomposite containing several nanocluster compositions. Although calcination is commonly used in the preparation of Pt–Sn catalysts, these results suggest that oxidative thermal treatments should be avoided to minimize phase separation of the desired catalyst composition.

Acknowledgements

This report is based upon work supported by, or in part by, the US Army Research Office under grant numbers DAAH04-95-1-0146 and DAAG55-98-1-0362. C.M.L. is grateful for this support.

References

[1] (a) C.M. Lukehart, S.B. Milne, S.R. Stock, Chem. Mater. 10 (1998) 903. (b) J.P. Carpenter, C.M. Lukehart, S.B. Milne, S.R. Stock, J.E. Wittig, B.D. Jones, R. Glosser, J.G. Zhu, J. Organomet. Chem. 557 (1998) 121. (c) J.P. Carpenter, C.M. Lukehart, S.B. Milne, D.O. Henderson, R. Mu, S.R. Stock, Chem. Mater. 9 (1997) 3164. (d) J.P. Carpenter, C.M. Lukehart, S.B. Milne, S.R. Stock, J.E. Wittig, Inorg. Chim. Acta 251 (1996) 151. (e) C.M. Lukehart, S.B. Milne, S.R. Stock, R.D. Shull, J.E. Wittig, ACS Symp. Ser. 622 (1996) 195. (f) C.M. Lukehart, S.B. Milne, S.R. Stock, R.D. Shull, J.E. Wittig, Mater. Sci. Eng. A204 (1995) 176. (g) K.J. Burnam, J.P. Carpenter, C.M. Lukehart, S.B. Milne, S.R. Stock, B.D. Jones, R. Glosser, J.E. Wittig, Nanostructured Mater. 5 (1995) 155. (h) C.M. Lukehart, J.P. Carpenter, S.B. Milne, K.J. Burnam, Chemtech 23 No. 8 (1993) 29.

[2] (a) J.H. Sinfelt, Bimetallic Catalysts: Discoveries, Concepts, and Applications, Wiley, New York, 1983. (b) V. Ponec, Adv. Catal. 32 (1983) 149.

[3] W.R. Moser (Ed.), Advanced Catalysts and Nanostructured Materials, Academic Press, San Diego, 1996.

[4] (a) J.A. Rodriguez, T. Jirsak, S. Chaturvedi, J. Hrbek, J. Am. Chem. Soc. 120 (1998) 11149. (b) Y.L. Tsai, B.E. Koel, Langmuir 14 (1998) 1200. (c) F. Humblot, D. Didillon, F. Lepeltier, J.P. Candy, J. Corker, O. Clause, F. Bayard, J.M. Basset, J. Am. Chem. Soc. 120 (1998) 137. (d) J. Szanyi, M.T. Paffett, J. Am. Chem. Soc. 117 (1995) 1034. (e) J.W. Peck, B.E. Koel, J. Am. Chem. Soc. 118 (1996) 2708. (f) C. Xu, J.W. Peck, B.E. Koel, J. Am. Chem. Soc. 115 (1993) 751.

[5] (a) J. Arana, P. Ramirez de la Piscina, J. Llorca, J. Sales, N. Homs, Chem. Mater. 10 (1998) 1333. (b) J. Llorca, P. Ramirez de la Piscina, J.L.G. Fierro, J. Sales, N. Homs, J. Catal. 156 (1995) 139. (c) I.B. Yarusov, E.V. Zatolokina, N.V. Shitova, A.S. Belyi, N.M. Ostrovski, Catal. Today 13 (1992) 655. (d) R. Srinivasan, L.A. Rice, B.H. Davis, J. Catal. 129 (1991) 257. (e) R. Srinivasan, L.A. Rice, B.H. Davis, J. Catal. 129 (1991) 257. (f) R. Srinivasan, R.J. De Angelis, B.H. Davis, J. Catal. 106 (1987) 449. (g) R. Burch, L.C. Garla, J. Catal. 71 (1981) 360.

[6] J. Llorca, P. Ramirez de la Piscina, J. Sales, N. Homs, J. Chem. Soc. Chem. Commun. (1994) 2555.

[7] C. Eaborn, A. Pidcock, B.R. Steele, J. Chem. Soc. Dalton Trans. (1976) 767.

[8] (a) H.P. Klug, L.E. Alexander, X-ray Diffraction Procedures for Polycrystalline and Amorphous Materials, second ed., Wiley, New York, 1974. (b) W.P. Halpwerin, Rev. Mod. Phys. 58 (1986) 533.

[9] T.B. Massalski, Binary Alloy Phase Diagrams, second ed., ASM International, Materials Park, OH, 1990.

[10] J.D. Kennedy, W. McFarlane, J. Chem. Soc. Perkin Trans. II (1974) 146.

[11] (a) T. Adachi, S. Sakka, J. Mater. Sci. 22 (1987) 4407. (b) C.J. Brinker, G.W. Scherer, Sol–Gel Science, Academic Press, New York, 1990.